THE ASTROPHYSICAL JOURNAL, 464:1016–1029, 1996 June 20

Hα SURGES AND X-RAY JETS IN AR 7260

RICHARD C. CANFIELD, KEVIN P. REARDON,[1] AND K. D. LEKA[2]
Institute for Astronomy, University of Hawaii, 2680 Woodlawn Drive, Honolulu, HI 96822
K. SHIBATA AND T. YOKOYAMA
National Astronomical Observatory of Japan, Mitaka, Tokyo 181, Japan
AND
M. SHIMOJO
Department of Physics, Tokai University, 1117 Kitakaname, Hratuka, Kanagawa, Japan
Received 1995 August 11; accepted 1996 January 8

ABSTRACT

We discuss nine events, observed simultaneously as jets in X-rays and surges in Hα, which are associated with moving magnetic bipoles. The X-ray jets share many features with those discovered by *Yohkoh* in active regions, emerging flux regions, and X-ray bright points (see paper by Shibata et al.); in particular, they originate near one end of a pair of small flaring loops. The Hα surges are adjacent to the X-ray jets. At the bases of these surges we observe both blueshifts (initially) and redshifts (1–2 minutes later). All the observed surges spin in a sense consistent with the relaxation of the twist stored in the magnetic fields of the moving magnetic bipoles. Newly discovered phenomena include footpoint convergence and moving-blueshift features.

We develop a model of the role of magnetic reconnection in these events. This model explains the temporal and spatial relationship between the jets and surges, the role of the moving bipoles, the flaring X-ray loops and their converging Hα footpoints, the Hα moving-blueshift features, the direction and amount of spin of the surges, and the relative temporal development of the Hα redshifts and blueshifts.

Subject headings: Sun: corona — Sun: magnetic fields — Sun: X-rays, gamma rays — sunspots

1. INTRODUCTION

X-ray jets were discovered using the Soft X-ray Telescope (SXT) of *Yohkoh* (Tsuneta et al. 1991). They have the following characteristics (Shibata et al. 1992a; Shibata, Yokoyama, & Shimojo 1994; Shimojo 1994): (1) They are extended linear structures whose length is much greater than their width; (2) the length ranges from 5×10^3 to more than 3×10^5 km, and the average is 1.7×10^5 km; (3) the peak translational velocity is usually between 30 and 300 km s^{-1}, and the average is 190 km s^{-1}; (4) almost all X-ray jets are associated with small flares in X-ray bright points, emerging flux regions, and active regions; (5) some X-ray jets show whiplike motion, i.e., the linear structure is not rigid; part of such jets move perpendicular to the direction of elongation at a few 10 s of km s^{-1}.

Hα surges have been studied for over 50 years (see Roy 1973a, b). They are straight or slightly curved ejections that reach peak velocities of 50–200 km s^{-1}. They reach heights of up to 200 Mm and typically last 10–20 minutes. The surge material either fades or returns into the chromosphere along the trajectory of ascent (Svestka 1976; Tandberg-Hanssen 1977; Foukal 1990). At high resolution, it is evident that the Hα structure of surges is highly filamentary (Roy 1973a; Zirin 1988, pp. 296–301). Surges show homology, pulsing behavior, and occur at the boundaries of magnetic field concentrations (Roy 1973a). They are associated with *satellite sunspots*, which are small spots of opposite polarity in or near the main spot's penumbra (Bumba 1960; Rust 1968), and moving magnetic features (Gaizauskas 1983). Sunspot growth and evolution (e.g., decay) both seem to be important factors in the production of surges (Roy 1973a).

Both Rust (1968) and Roy (1973a) proposed that reconnection of magnetic fields near a coronal neutral point above satellite spots accounts for surges. Kurokawa & Kawai (1993) showed that Hα surges are seen in the early stages of flux emergence and concluded that they are produced by magnetic reconnection between the emerging flux region and the preexisting surrounding region. These ideas are strongly supported by the reconnection model developed below.

It was first thought that Hα surges were not associated with X-ray or EUV emission (see, e.g., Rust, Webb, & MacCombie 1977). This result, however, was strongly biased by the insensitivity of the X-ray instruments used in the comparisons. Numerical modeling of magnetohydrodynamic reconnection (Shibata, Nozawa, & Matsumoto 1992b; Yokoyama & Shibata 1995) strongly implies that one should expect the acceleration of both hot (X-ray) and cold (Hα) plasmas.

For some time it has been clear that the phenomenon we call surges in Hα and jets in X-rays can be seen at many wavelengths and are closely related in certain types of events. From ATM/*Skylab*, Schmahl (1981) found that surges could be seen in the Extreme Ultraviolet. There exist numerous *Solar Maximum Mission* observations of X-ray events related to surges, which are summarized by Svestka, Farnik, & Tang (1990) and Schmieder et al. (1993). X-ray observations with the NIXT rocket (Schmieder, Golub, & Antiochos 1994) allowed tests that strongly constrained, but did not rule out, pressure-driven models of surges. Using the HRTS rocket, Korendyke et al. (1995) observed a surge

[1] Present address: Osservatorio Astronomico di Capodimonte, via Moiariello 16, 80131 Napoli, Italy.
[2] Present address: High Altitude Observatory, NCAR, P.O. Box 3000, Boulder, CO 80307-3000.

at very high resolution in the EUV showing fine structure, comparable to what is observed in Hα.

Models of surges and jets can be classified according to the driving force: gas pressure, shock wave, magnetic tension force, and magnetic pressure (both twist and "melon-seed" type). Models driven by gas pressure or external force have been studied by Steinolfson, Wu, & Schmahl (1979), Karpen et al. (1982), Shibata et al. (1982), and Sterling, Shibata, & Markiska (1993). The gas-pressure models assume a sudden thermal energy release at the top of the chromosphere. If thermal energy release occurs deep in the chromosphere, shock waves can be important (Shibata et al. 1982; Sterling, Shibata, & Mariska 1993). The influence of the magnetic tension force has been studied, e.g., by Pikel'ner (1969), Blake & Sturrock (1985), Yokoyama & Shibata (1994, 1995), and Heyvaerts, Priest, & Rust (1977). This force results from reconnection and gives rise to the slingshot effect. Models in which twisted magnetic field lines are the driving force have been advanced by Shibata & Uchida (1986) to explain surges and by Hollweg, Jackson, & Galloway (1982) to explain spicules. Melon-seed models were proposed by Livshits & Pikel'ner (1964), Uchida (1969), Shibata et al. (1992b), and Yokoyama & Shibata (1994).

Throughout this paper we follow the convention used above: the term "surges" refers to the phenomenon seen in Hα and "jets" to that seen in X-rays. In § 2 we discuss how the instruments aboard the *Yohkoh* satellite (Ogawara et al. 1991) and at Mees Solar Observatory have been used to make unique cotemporal observations of jets, surges, and magnetic fields. The observations themselves are described in § 3. Finally, in § 4 we interpret our observations through a phenomenological reconnection model in which magnetic tension and relaxation of magnetic twist play a dominant role.

2. INSTRUMENTATION AND DATA REDUCTION

The SXT (Tsuneta et al. 1991) observes the Sun in the wavelength range 3–50 Å with an instrumental pixel size of 2.″5. The image cadence ranges from seconds (in "flare mode": 160″ × 160″ field of view) to minutes (in "quiet mode": 320″ × 320″ images) between successive frames with identical observing parameters. All SXT images in this paper were taken through the thin aluminum (Al.1) filter, at various levels of resolution (full, half, quarter) corresponding to 2.″5, 5″, or 10″ pixel size. An aspect telescope provides narrowband optical images, which we use to coregister the SXT images data with ground-based data.

The Mees Solar Observatory data consist of digital Hα filtergrams, spectroheliograms, and spectra from the Mees CCD Imaging Spectrograph (MCCD) and photospheric vector magnetograms from the Imaging Vector Magnetograph (IVM).

The MCCD (Penn et al. 1991) obtains digital spectroheliograms in the spectral range Hα ± 10 Å by scanning the solar image from a 25 cm coudé coronagraph telescope across a spectrograph slit. All pixels in the spectral dimension and one spatial dimension (along the spectrograph slit, terrestrial north-south) are sampled simultaneously; the other spatial dimension is built up sequentially. The resultant data have 2.″4 pixel^{-1} spatial and 0.37 Å pixel^{-1} spectral resolution across a 230″ × 290″ field of view. An Hα image, obtained through an interference filter of bandwidth about 1 Å, is digitized from a video-rate CCD camera with a larger field of view and smaller spatial pixel size (≈0.″5 pixel^{-1}) than the spectroheliograms. The sampling cadence (time to return to the same point on the Sun) is 21 s. Doppler velocities are calculated from the shift of the Hα absorption line center. Hα spectroheliograms are made at line center, which varies in wavelength due to these shifts.

The IVM (Mickey et al. 1996) uses a Fabry-Perot etalon to obtain images at various wavelengths across an appropriate spectral line and in the nearby continuum. For our observations we used nine positions at 36 mÅ spacing across the 6302.5 Å line and a continuum position near 6302.0 Å. On-chip binning resulted in 256 × 256 pixels of 1.″1 dimension, although spherical aberration in the telescope during these observations (made early in the development of the IVM) limited the true resolution to approximately 3″. The IVM data were reduced from polarization signals to a magnetic flux map using the derivative method (Jefferies, Lites, & Skumanich 1989; Jefferies & Mickey 1991).

The *Yohkoh* and Mees data are coregistered, using white-light images, with a spatial accuracy that is typically a few arcseconds, and have an instrumental temporal accuracy that is much better than 1 s. Given the 21 s cadence of the Mees data, there is a time difference of at most 10.^{s}5 between a given X-ray image and the closest Hα observation.

3. OBSERVATIONS

NOAA AR 7260 has been described extensively in previous studies of flux emergence, owing to its good observational coverage by *Yohkoh* and Mees. Leka et al. (1994; henceforth Paper I) have systematically described its structure and evolution, and we refer to this paper for both its nomenclature and its discussions of moving satellite spots, penumbral filaments, and emerging flux. Figure 18 of that paper provides an Hα overview of the satellite spots and penumbral filaments associated with the large preceding-polarity (negative vertical magnetic field) sunspot called P0α; these features are closely related to the jets and surges studied in this paper. Leka et al. (1996; henceforth Paper II) have studied sunspot motions, X-ray loop and Hα fibril morphology, and vector magnetic fields in this region. They find that all structures for which these quantities can be observed have the same sign of magnetic helicity, which is clearly shown in the vorticity of the Hα fibrils and X-ray loops in the Paper I figure. For our study we selected the Hawaii observing day spanning 1992 August 19–20 (UT), when the large leader spot (termed PO α in Paper I) was at approximately N16 W30. During this time period AR 7260 was very productive of events seen as X-ray jets by SXT and Hα surges at Mees Solar Observatory, which we have chosen to study in this paper.

Table 1 lists all observed properties of the nine simultaneous X-ray jet and Hα surge events studied, each identified by a reference time (UT); each of these listed properties is discussed individually in the appropriate section below. As noted below, the X-ray jets vary widely in their intrinsic brightness, as well as the cadence and spatial resolution (from 2.″5 to 10″ pixel size) with which they were observed. Hence it is possible to infer all properties listed for some events—those which are brightest and best sampled in X-rays, such as the events of 21:40 and 23:11 UT. It is not possible to do so in other less well sampled events (e.g., 02:36), for which many blank entries (*ellipsis dots*) appear; a question mark (?) indicates uncertainty, an exclamation

TABLE 1

PROPERTIES OF OBSERVED JETS/SURGES

PARAMETER	REFERENCE TIME (UT)								
	1730	1834	2140	2212	2311	0027	0224	0236	0237
Position angle	0°	80°	0°	80°	0°	70°	0°	0°	15°
X-ray loop(s) observed?	No[a]	No[b]	Yes	No[c]	Yes	Yes	Yes	Yes	Yes
Hα loop(s) observed?	Yes	Yes[d]	?	Yes	Yes	Yes	No	No	...
Number of Hα footpoints	3	3?[e]	3	2	3	2	?	?[f]	?[f]
Initial Hα brightening location	?	?	S	?	N	?	?	?	...
Brightest Hα loop location	?	N[g]	?	...	N	...	?	?	?
Brightest Hα footpoint location	N	N[g]	S	N	N/M	N	N	?	?
Number of X-ray loops	...	...	2[h]	...	2[h]	2	2?	1	1
Initial X-ray brightening location	...	...	NF	...	NF	SL	NL	...	...
Brightest X-ray loop	...	...	S	...	S	S	N?	...	...
Brightest X-ray footpoint	...	...	N	...	N	...	...	...	...
−/+/− polarity pattern observed?	Yes?	Yes?	Yes?	Yes?	Yes	Yes	Yes	Yes	Yes
Hα surge bright?	Yes	Yes!	Yes	Yes	Yes	Yes	?	?	?
Helical Hα surge structure?	Yes?	Yes?	Yes?	?	Yes?	Yes?	Yes?	?	?
Surge spin handedness	R	R	R	R?	R	R	R	R	?
Hα downflow at surge base?	Yes	Yes	Yes	Yes?	Yes	Yes	No	No	No
Hα downflow begins after upflow?	Yes	Yes	Yes	Yes?	Yes	Yes	...	...	No
Surge location over outer loop?	Yes	Yes	Yes	Yes?	Yes	Yes?	Yes	Yes	?
Moving blueshift feature observed?	No	Yes[i]	No	Yes	No	Yes[j]	No	No	No
Blueshift observed above loops?	No	Yes	No	Yes	Yes	Yes	...	Yes	...
Multiple velocity episodes?	Yes	Yes	Yes	?	Yes	Yes	Yes	No	?
Approaching Hα footpoints?	No	Yes!	Yes	Yes	No	No	No	No	No

[a] Only one X-ray point-no structure.
[b] Only one X-ray image exists.
[c] Only part of jet is in PFI, hard to judge.
[d] Best example of whiplike motion.
[e] Short-lived blueshift point.
[f] Poor seeing; cannot tell.
[g] N means outermost footpoint.
[h] Actually three footpoints, not two loops.
[i] Moving blueshift both before and after.
[j] Best example of moving blueshift event.

mark (!) indicates a very strong effect. The event's position angle given in the table is measured relative to a line extending solar northward from the upper half of POα, in a clockwise direction.

The characteristic of the satellite spots surrounding P0α that is most relevant to our study is their motion away from the central spot into the surrounding active region and plage magnetic field, accompanied by the slow separation of their conjugate footpoints. This motion is strikingly shown in Figure 1, which tracks numerous satellite spots of both polarities during the 8 hr period studied. The labeled satellite spots are associated with two particular events, which are discussed at length below because they best illustrate properties observed in many of the events. The bipole pair associated with the 23:11 event shows typical outward motion and conjugate-polarity divergence. Both Hα and X-ray loops indicate that these satellite spots are magnetically connected and associated with this event. Their motion is most simply understood in terms of an Ω-shaped bundle of magnetic flux tubes that is emerging into the corona from beneath the photosphere, adjacent to P0α.

Our data lack sufficient spatial resolution to be able to resolve fully some well-known morphological features of surges, e.g., filamentary or helical structure. Nonetheless, what appears to be underresolved helical structure is often seen, which supports the idea that they occur in nonpotential magnetic structures. We also find that most of the surges tend to be bright in Hα at some point in their lifetime, although evidence presented below implies that this is just a Doppler-brightening effect (see, e.g., Hyder & Lites 1970; Heinzel & Rompolt 1987).

We now turn to the two events that best illustrate the key properties detailed in Table 1. The 23:11 UT event most clearly shows that the bright flaring X-ray source consists of two loops and is associated with a magnetic polarity inversion, the surges spin around their axes, and the Hα upflows and downflows have distinctive temporal and spatial interrelationships. However, the surge and the jet appear to be in a plane nearly parallel to the line of sight in this event, so projection effects make it hard to infer their relationship in three dimensions. This problem does not exist in the 18:34 event, in which the surge and jet are viewed more laterally. This event best shows that field lines undergo whiplike motions, the loci of bright Hα footpoints approach each other as the event progresses, and the jet and the surge are not cospatial.

3.1. *The 23:11 UT Event*

This event produced the longest and brightest X-ray jet in our data set, as shown in the right panel of Figure 2. X-ray jets commonly emanate from flaring X-ray structures or X-ray bright points (Shibata et al. 1992a), as this one does. However, the flaring X-ray structure (the brightest X-ray feature) is not a single loop, as it seems to be in Figure 2; its appearance in this image is strongly affected by image saturation. Evidence that it consists of two loops, end to end, is shown in Figure 3. Only in the saturated image at 23:12:37 UT does it appear as a single large loop; the other images

1996ApJ...464.1016C

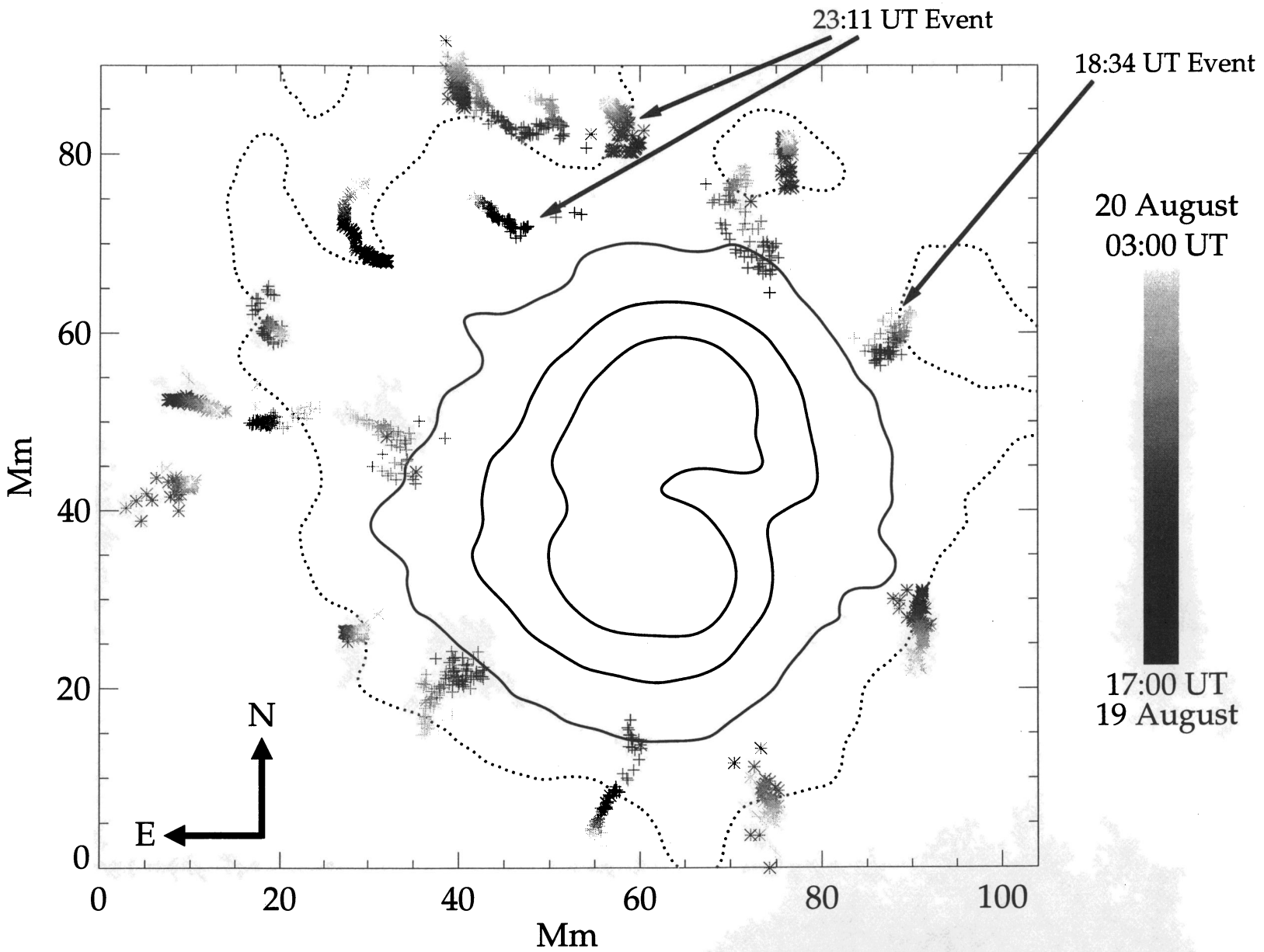

FIG. 1.—Motions of satellite spots around P0α. Locations of centers of the satellite spots at times between 17:00 on August 19 and 03:00 on August 20 (UT) are marked with asterisks and plus symbols for positive and negative polarity, respectively. The darkest symbols indicate the earliest times. The solid contours of continuum brightness outline P0α. The dotted contours are the average locations of the vertical-field polarity inversion line. Solar north is up, east to the left, and distances are measured in a plane tangent to the solar surface in all figures.

1996ApJ...464.1016C

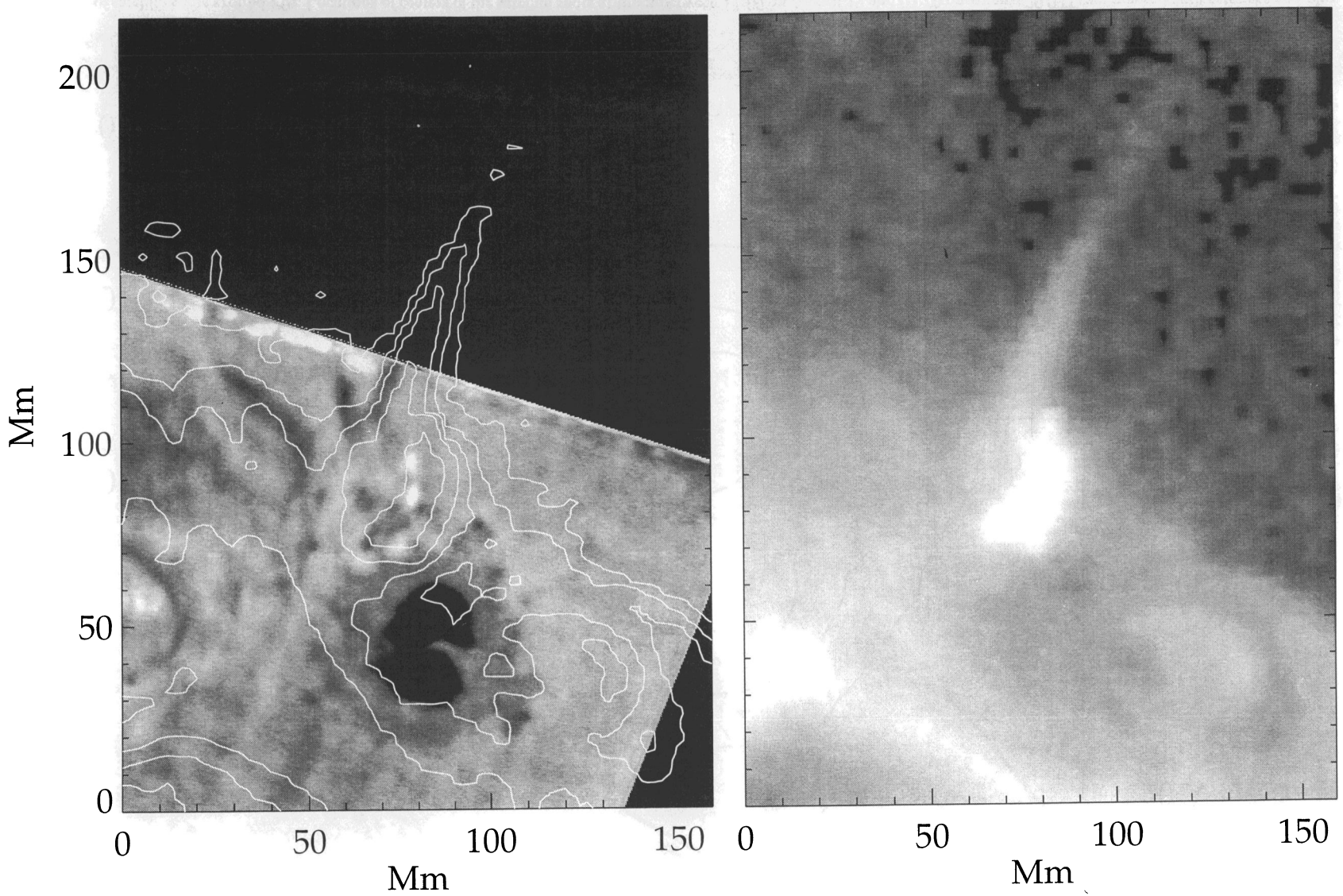

FIG. 2.—Images of the 23:11 event. *Right*: a portion of the *Yohkoh* SXT full-disk image of 23:16:57, 5″ pixels. *Left*: contours of this SXT image overlaid on the Mees Solar Observatory Hα filtergram of 23:16:54. The black area is outside the field of view of the filtergram.

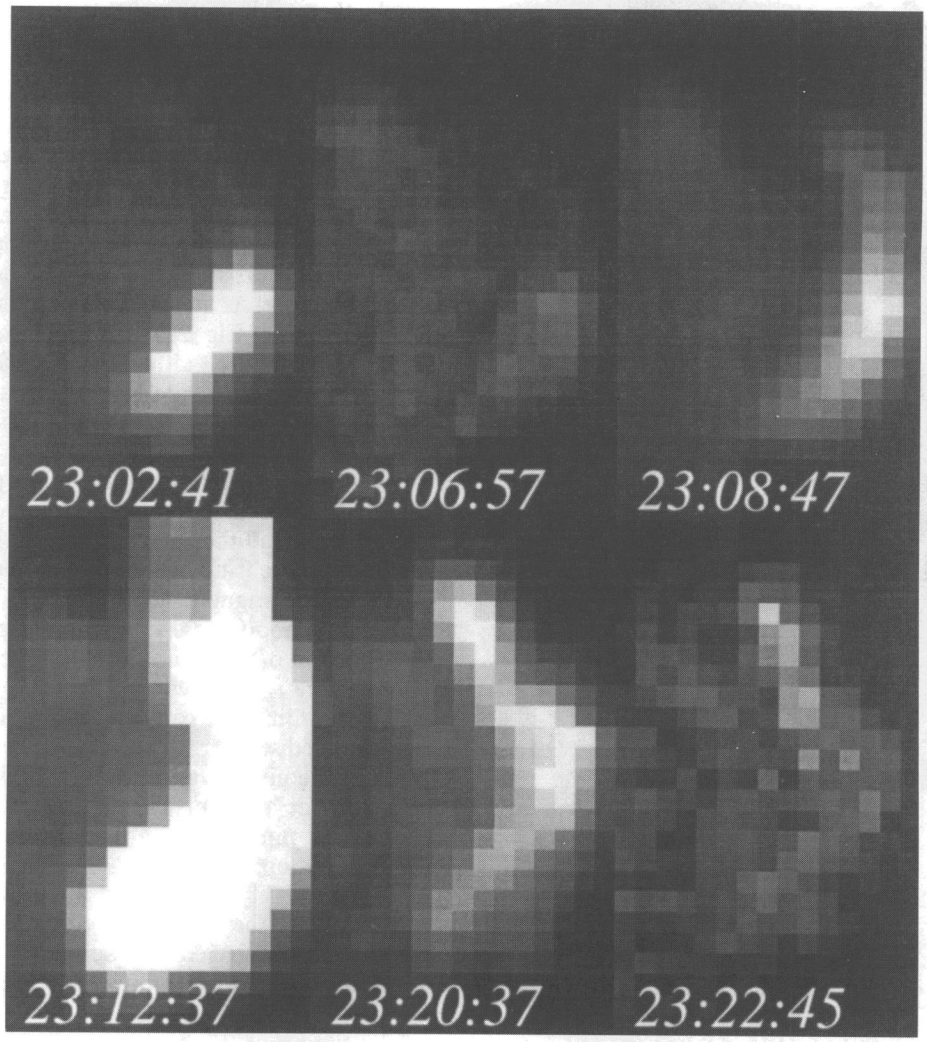

FIG. 3.—Full-resolution SXT images of the flaring X-ray structure of the 23:11 event. The image at 23:12:37 UT is saturated.

clearly show that the upper and lower parts often have different brightness. Moreover, the upper and lower parts have different light curves during the 23:11 event itself. Figure 4 divides the flaring region into five parts, as shown. The light curves of these regions are significantly different. These images and light curves show that the flaring X-ray structure consists of two loops that are contiguous, end to end.

The overlay of a broadband Hα image and X-ray contours in the left panel of Figure 2 shows the relationship of the X-ray structures to the large spot P0α and other features in a broadband Hα filtergram. One can see three bright Hα features along the western edge of the flaring X-ray structure, which we identify as the footpoints of the two X-ray loops. The upper one is the northern footpoint of the northern X-ray loop, the middle one is where the northern and southern X-ray loops essentially touch, and the lower one is the southern footpoint of the southern X-ray loop. The southern and central bright features are near the two satellite spots identified with this event in Figure 1. However, they do not coincide exactly, showing that this event does not occur at the site of greatest magnetic field strength. No satellite spot is seen at the northern footpoint.

In the filtergram in Figure 2, the Hα event appears as two nearly parallel dark surges (visible only near the base of the X-ray jet, owing to the edge of the field of view); one of them coincides spatially with one edge of the X-ray jet, the other does not. We attach little significance to the near coincidence of this surge and jet, for two reasons. First, the jet/surge and the closed loops appear to be located in a plane that is nearly parallel to the line of sight; such structures appear to coincide from such a viewing angle. Second, filtergrams show Hα-absorbing material in only a narrow range of radial velocities. In agreement with Xu, Ding, & Yin (1984), we believe that this causes the Hα surges to appear significantly narrower in our filtergrams (Fig. 2) than in our imaging spectra (per Fig. 6 discussion below). Finally, the fact that two surges appear in Hα, but only one jet appears in X-rays, suggests a large variation in the relative amounts of hot and cool plasma. This idea is supported by the study of Schmieder et al. (1995), all of whose events were seen as surges in Hα and bright loops in X-rays, but none of which were accompanied by X-ray jets bright enough to be observed by SXT.

All the observed events occur in association with satellite sunspots and bipolar magnetic features, and span two vertical-field polarity inversion lines, a characteristic of surges discovered by Rust (1968). The vertical-field magnetogram of Figure 5, coregistered and overlaid with an X-ray image of the 23:11 event, illustrates this relationship. The

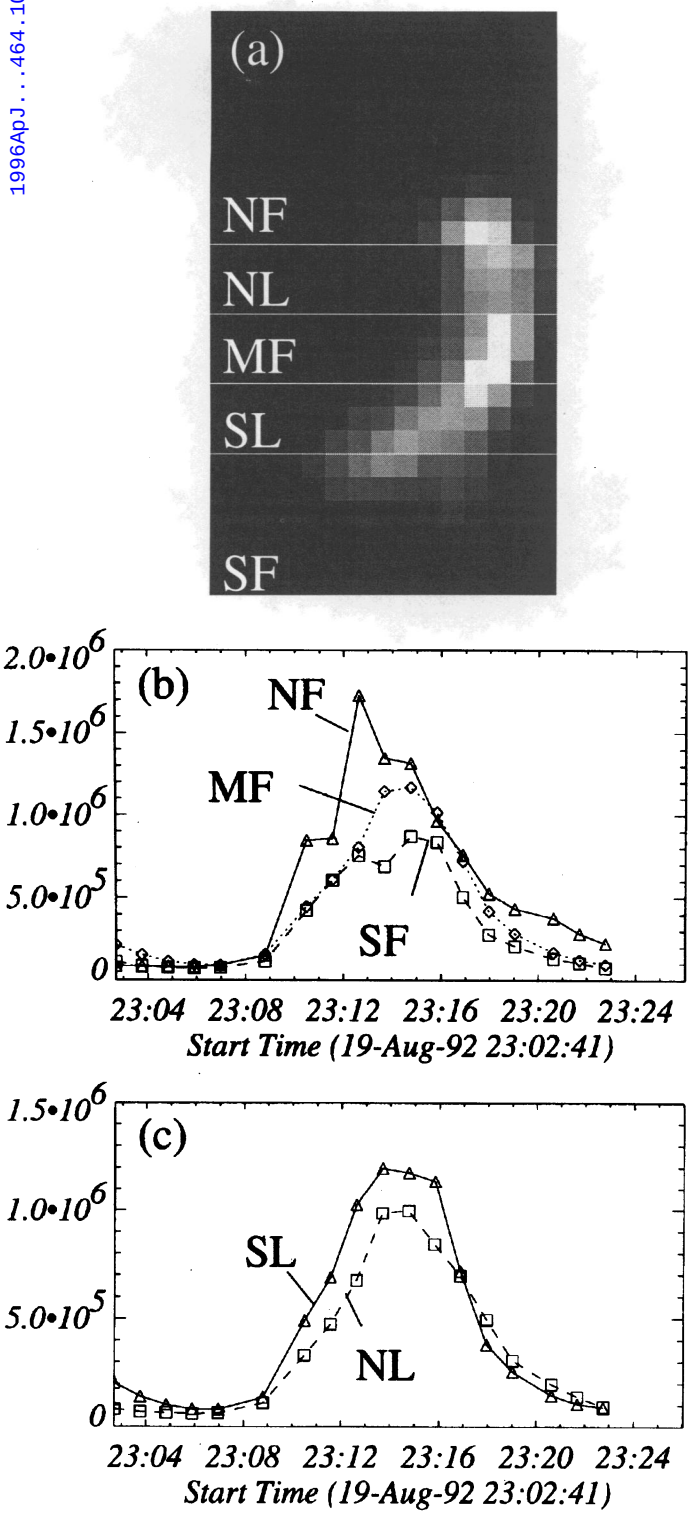

FIG. 4.—SXT light curves of regions within the flaring X-ray structure of the 23:11 event. (*a*) Definitions of the areas used for the light curves; the lines define the edges of the areas. (*b*) Light curves for the north, middle, and south footpoints. (*c*) Light curves for the north and south interfootpoint regions.

southern end of the flaring X-ray feature is in a region of negative polarity, near one of the moving satellite spots shown in Figure 1. The central part of this feature is in a region of positive polarity, near another moving satellite spot, also shown in Figure 1. Finally, the northern end is in a region of negative polarity and weaker field; no spot is visible there. All of the events in Table 1 show clear or probable association with this characteristic alternating pattern of magnetic polarities.

It is well known (Öhman, Hosinsky, & Kusoffsky 1968; Xu, Ding, & Yin 1984; Gu et al. 1994) that surges spin as they are ejected outward. Figure 6 shows Hα velocity contours overlaid on an Hα spectroheliogram and X-ray contours at a time (about 23:11:30) during the 23:11 event at which the surge and jet are well developed. The black X-ray intensity contours show the jet at the north tip of the flaring X-ray structure. As an aside, we note that (in contrast to the Hα filtergram of Fig. 2) the Hα spectroheliogram shows no surgelike structure, although the Hα velocity contours (*dashed and dotted white curves*) reveal the location of the 23:11 surge due to its rotational motion. Clearly the spinning surge is much wider in extent in the Hα velocity contours in Figure 6 than it is in the simple Hα filtergrams of Figure 2, as discussed above. Three points are noteworthy and typical of all the surges observed. First, uniform spin is observed; there is no evidence of filamentation. Second, the characteristic angular rate of this spin is about 10^{-3} radian s^{-1}, lasting about 1000 s. Third, the spin is right-handed, if the direction of the thumb is chosen to be upward from the photosphere. As shown in Table 1, all those surges for which the direction can be determined spin in this same right-handed sense.

Six of the nine surge/jet events show highly localized Hα downflow at a bright point at the base of the surge, and eight of the nine events show that the surge is located over the outer loop, which is called the northern loop in the table. The 23:11 event, shown in Figure 6, is typical in both respects: first, the downflow region (*dashed white contours*) is located at the base of the surge; second, it is at the north footpoint of the north loop, i.e., the footpoint farthest from P0α.

The timing of this highly localized Hα downflow is distinctive. The 23:11 event, whose velocity curves are shown in Figure 7, is typical. For ease of discussion, we have defined three stages based on velocity and X-ray emission properties. During stage 1, blueshifts (*lower panel*) gradually develop; they do so at least 10 minutes before they peak. The fact that Hα gradually brightens ("+" *curve*) during this same time period, although no X-ray brightening is seen (*starry curve*), supports the idea that this is Doppler brightening. Then, during stage 2, Hα brightens dramatically and X-ray emission begins to increase. Finally, in stage 3, X-rays peak and a strong redshift appears and peaks with a delay of about 1 minute with respect to the time of peak blueshift. As Figure 6 shows, this redshift is not cospatial with the strong blueshifts, which arise in surge, but rather originates in the highly localized region at the surge base. Most of the events in Table 1 have the characteristic that Hα downflow is seen at the surge base and this downflow begins after the upflow in the surge. Finally, the value of the peak velocity in all events tends to fluctuate in a bursty and episodic manner, like that of the 23:11 event shown in Figure 7.

3.2. *The 18:34 UT Event*

The 18:34 event is revealing because, in contrast to the 23:11 event, it appears to occur in a plane that is considerably inclined to the line of sight. Although we have only a single low-resolution X-ray image of this event, it shows an obvious linear structure extending from a bright base (white

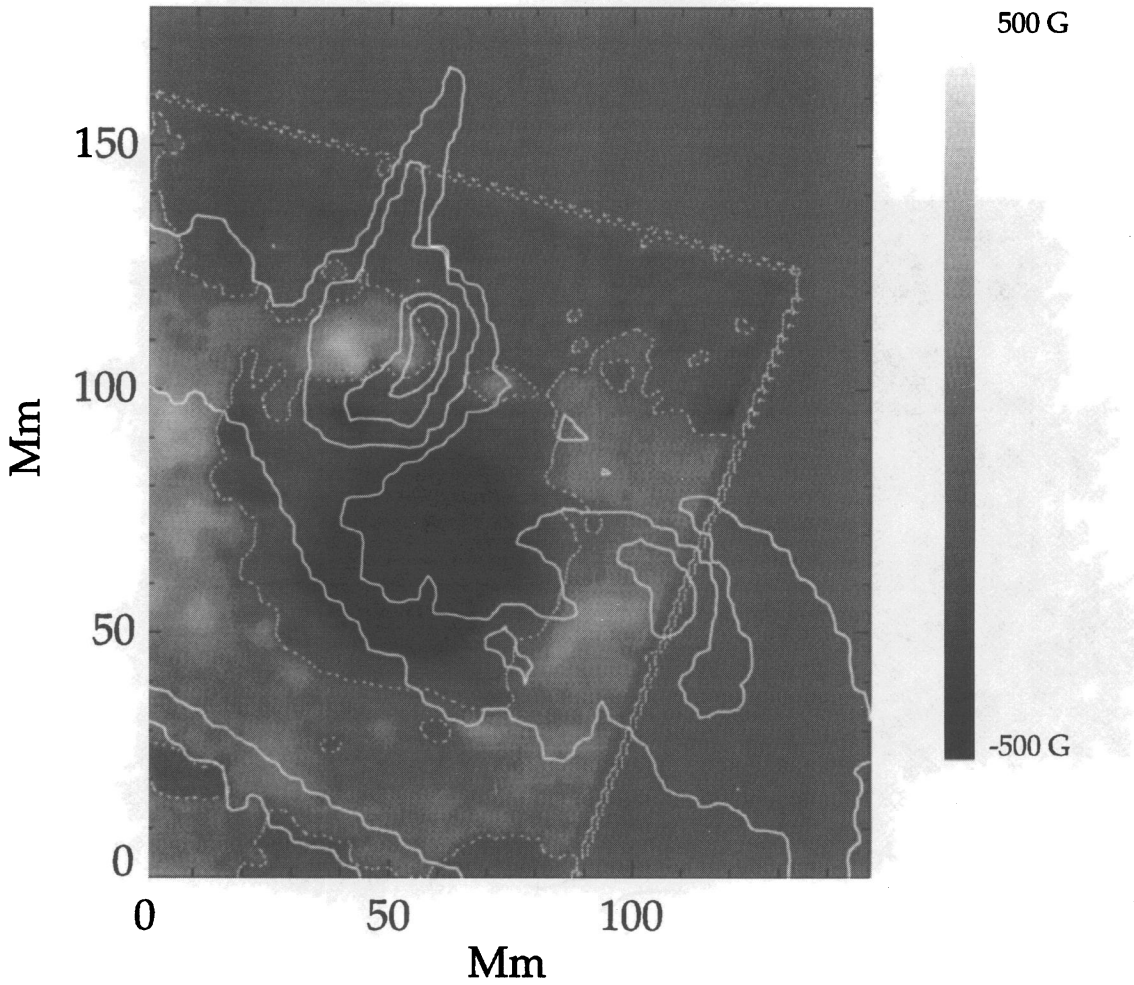

FIG. 5.—Magnetic context of the X-ray jet of 23:11. The half-tone image is the vertical magnetic field derived from the IVM magnetogram of 23:51, using the scale at the right. Polarity inversion contours are indicated by short-dashed lines. SXT intensity contours are indicated by the solid white curves. The linear artifacts are produced at the edges of the magnetogram.

contours in Fig. 8), properties that we associate with a jet. The northwest quadrant of the figure shows both the surge (dark in the underlying Hα spectroheliogram) and the jet as long linear structures. Despite the low X-ray resolution, it is clear that they are *not* cospatial; the Hα surge appears above the X-ray jet.

The Hα light curve, shown in the upper part of Figure 9, provides a useful reference for this event. Like the 23:11 event, this one shows blueshifts (not shown) beginning more than 15 minutes before the Hα velocity peaks. However, the redshift at the surge base (black dashed contours in Fig. 8) has a more gradual onset and neither the maximum redshifts nor the maximum blueshifts are as erratic or impulsive. The strips of images in the lower part of Figure 9 show interesting phenomena in the rectangular region at the base of the surge and jet, as defined by the rectangular box between the surge and P0α in Figure 8, during the three interesting periods of time indicated by A, B, and C.

The series of Hα spectroheliograms during time period A shows two small penumbral filaments over a period of about 2 minutes during the initial Hα intensity rise. At the beginning of the time series one penumbral filament is more curved than the other, suggesting that they are intertwined. The end of the less strongly curved penumbral filament farthest from P0α rears up in a whiplike manner, while the other end remains in place. Other events in this sector northeast of P0α, called M4 in Paper I, also show this whiplike motion in Hα, and such motions are a clue about the effects of reconnection.

The series of Hα line-center spectroheliograms during the time period B, which leads up to Hα maximum, shows two brightenings whose motions are of interest. The two sites of greatest brightness in the first image (18:29:02, see also 18:29:23 and 18:29:44 in strip A), which appear to be footpoints, approach one another, dramatically decreasing their separation until they almost touch (18:35:21). Such approaching bright points are seen in three of the nine events in Table 1. It is interesting that the direction of this motion is opposite that of the footpoint spreading seen in Hα ribbons (see, e.g., Svestka 1976) and hard X-ray footpoints (see, e.g., Sakao et al. 1992) in eruptive flares. The bright points converge at a speed of about 20 km s^{-1}. To our knowledge, this converging footpoints phenomenon has not been reported before.

The right-hand column of Hα velocity scans shown in time period C illustrates another phenomenon that, to our knowledge, has not been reported previously. A blueshifted (dark) linear structure appears in all images, moving from

1996ApJ...464.1016C

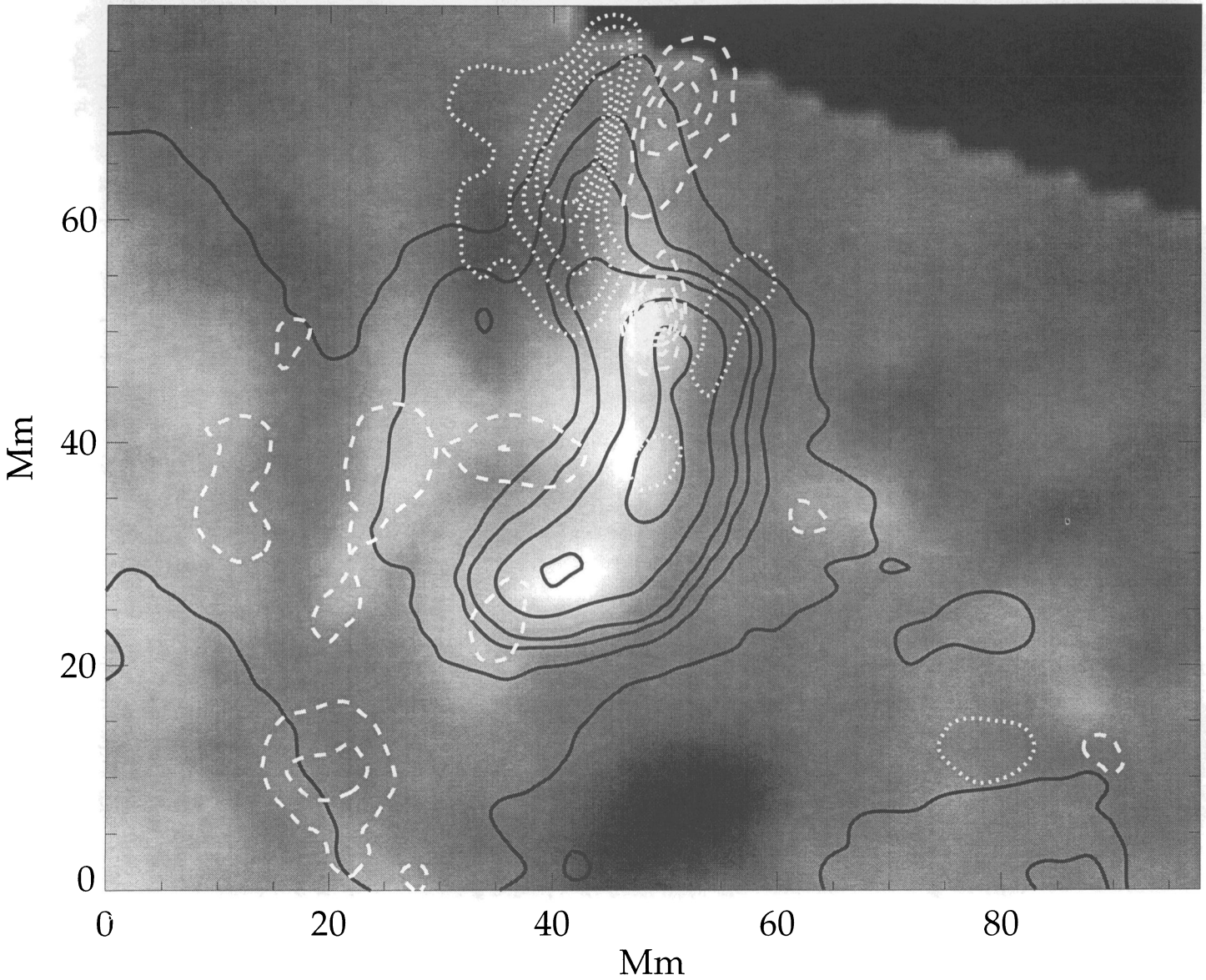

FIG. 6.—Dynamics of the Hα surge relative to the X-ray jet of 23:11. Contours show X-ray intensity from a half-resolution SXT image at 23:11:33 (*solid black*) and Hα redshift (*dashed white*) and blueshift (*dotted white*) from the MCCD scan made between 23:11:27 and 23:11:35. The half-tone image shows line-center Hα intensity.

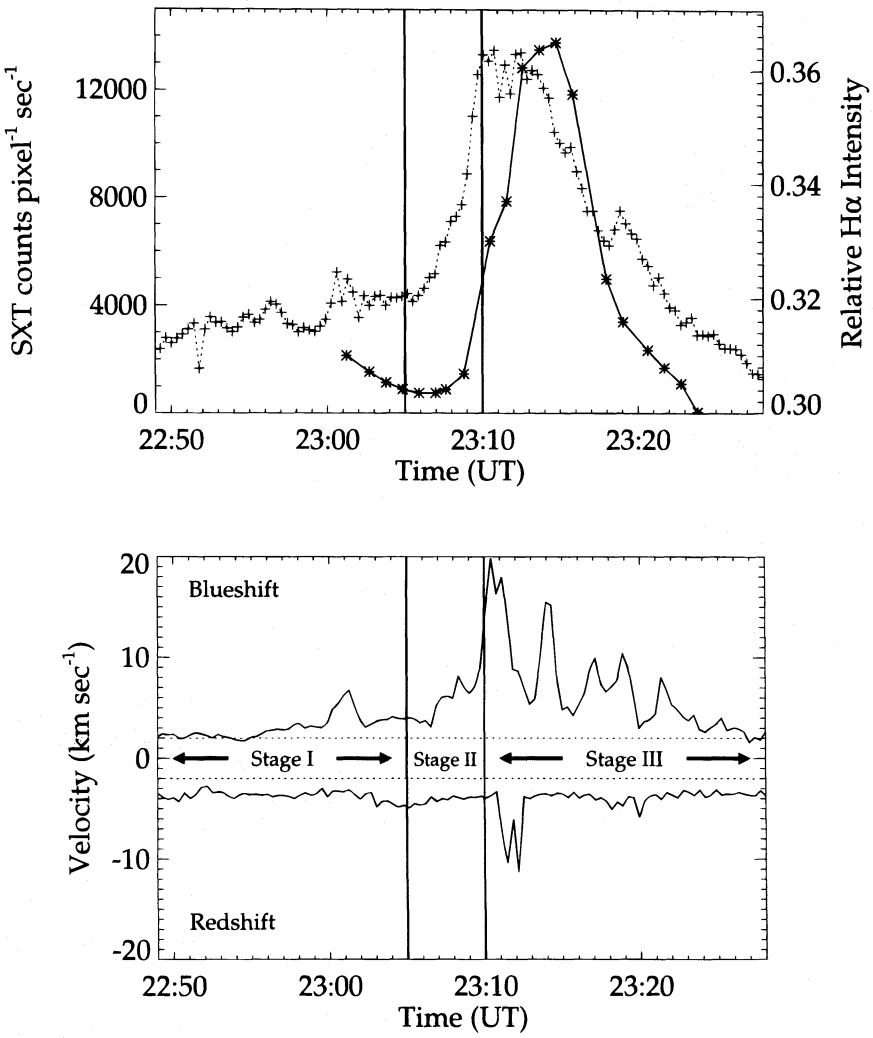

FIG. 7.—Hα brightness and radial velocity curves for a subarea of Fig. 6 that includes the surge and the bright flaring loops of the 23:11 event. *Top*: Hα line center (*plusses*) and X-ray intensity (*starry*) observations. *Bottom*: The maximum values of both redshift and blueshift in the selected subarea, as a function of time. The horizontal dashed lines indicate the 3 σ level of all velocities in the subarea. Stages 1, 2, and 3 are defined in § 3.1 and interpreted in § 4.1.

right to left along a path parallel to the penumbral filament that showed whiplike motion in strip A. The measured transverse speed of propagation of the blueshift region during the period of obvious motion shown in Figure 9 averages 25 km s^{-1} and peaks at 120 km s^{-1}. In the 18:34 event this *moving blueshift* phenomenon is seen both before and after the surge/jet event, but in several other events it is seen only before.

4. INTERPRETATION

We tie together our X-ray and Hα observations with a model of reconnection that links magnetic fields, motions, and time during the stages of development defined in Figure 7. This model depicts the role of reconnection in the spin of the surge, the Hα redshifts at its base, and the moving-blueshift phenomenon.

4.1. *Morphological Model*

The following morphological model, shown in Figure 10, depicts our interpretation of the phenomena that we have observed. Stage 1 represents the morphology before reconnection begins. Stage 2 shows the period of early reconnection, before strong heating. Stage 3 shows phenomena that occur after strong heating and reconnection have taken place.

In stage 1, the bipole associated with the moving satellite spots and Hα penumbral filaments is represented by the shaded area contained between the closed field lines that connect conjugate footpoints 1 through 4. During this stage this bipole moves away from P0α (northward) into the preexisting large-scale (open) magnetic field structure. This direction of the bipole's motion leads to reconnection at its leading (northern) side.

During stage 2, reconnection of field lines 1 to 2 takes place, and cool plasma moves in the directions indicated by the double arrows. In Figure 7, Hα brightens as the speed of the surge increases (Doppler brightening), but the gas between field lines 2 and 3 is only weakly heated to X-ray temperatures. The gas between field lines 1 and 2 is not heated significantly, but undergoes upward motion that is whiplike, i.e., the point of motion propagates along the field line, as seen in the simulations of Yokoyama & Shibata (1995). This whiplike motion leads to the moving blueshift events.

At the beginning of stage 3, strong heating begins, and the X-ray jet is vigorous. As observed, the Hα surge is above the

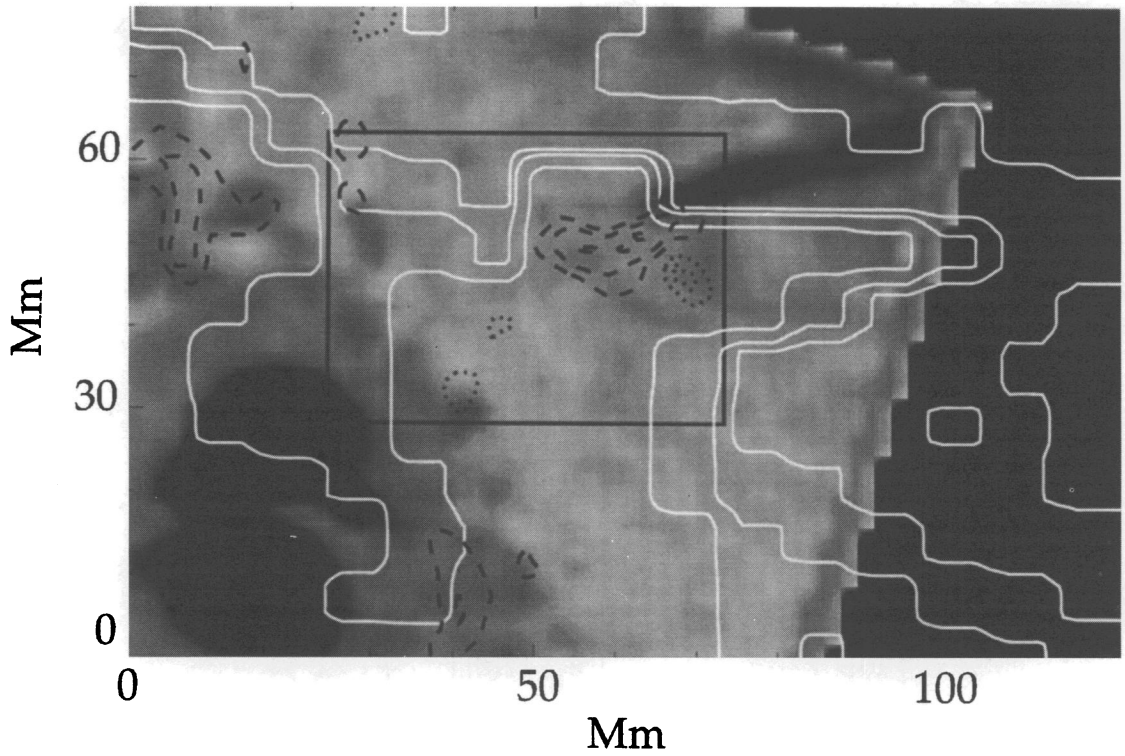

FIG. 8.—Dynamics and morphology of the 18:34 jet and surge. The white X-ray intensity contours are from a 668 ms quarter-resolution SXT exposure taken at 18:34:01. The half-tone image is portion of the Hα filtergram of 18:34:05. The dashed black contours indicate Hα redshift, dotted contours indicate blueshift. The spectroheliogram from which these Hα line shift contours come was taken between 18:33:59 and 18:34:05. The black rectangle defines the region displayed in Fig. 9.

jet. Bright X-ray loops are present, and strong Hα downflow occurs at the northern footpoint (indicated by the small rectangle and downward double arrows beneath the base of the quiet corona).

4.2. *The Spinning Motion of the Surges*

In our model, redistribution of stored twist leads to the spin of the surge material. The magnetic field of P0α is strongly twisted in a left-handed sense (Papers I and II). When this twisted field (1 and 2 in the closed loop on the south side of Fig. 10) reconnects with less twisted surrounding coronal field (1 and 2 on the north side), the twist stored in the closed loop field propagates up the reconnected field line, leading to spinning in the right-handed sense. Such release of stored twist is a surge mechanism suggested by Shibata & Uchida (1986).

The plausibility of this interpretation can be tested quantitatively using our data. The amount of stored twist can be estimated from the observed values of the force-free field parameter α and the length of the prereconnection field lines. The observed value of α in the moving magnetic bipoles near P0α is about 0.4 $(\mathrm{Mm})^{-1}$ (Paper II). The observed length of the penumbral filaments is $l \sim 20$ Mm, so the twist (of order αl) stored above the photosphere is several radians. The observed spin of the filaments typically proceeds at about 10^{-3} radians s^{-1} for approximately 10^3 s, corresponding to a total observed rotation of order 1 radian. Hence the data indicate that, to order of magnitude, enough twist is stored to explain the observed rotation.

Two alternative explanations for the spin are not supported by our observations. First, if the Hα surge material was merely moving along a static magnetic field structure of helical form, and we make the assumption that the structure has the same sense of twist as all other observed fields in the region (Papers I and II), the observed direction of spin would be opposite from what we find. Second, velocity profiles across the surges shows that they spin like single large cylinders, rather than a collection of many smaller parallel cylinders, each rotating about its own axis. We know that in Hα, filamented structure is typically observed when sufficient spatial resolution is available (see, e.g., Foukal 1990). Since our data show that Hα surges and X-ray jets are not generally cospatial or interleaved, these filamented structures can be explained only by contrast with their surroundings in density, not temperature. The observed spin profiles, like single large cylinders, thus argue against the ambipolar-diffusion mechanism of Gu et al. (1994), which is driven by density gradients.

4.3. *Upward and Downward Reconnection Jets*

As shown in Figure 10 (stage 3), upward and downward reconnection jets are expected above and below the reconnection site, respectively. In our interpretation, the upward jet is seen directly in X-rays, but the downward jet is not. Instead, we see only the consequence of the impact of the downward reconnection jet on the chromosphere, i.e., the small region of Hα downflow. Three aspects of the observations favor this interpretation, in contrast to the obvious alternative, i.e., that the redshifts are the reaction to the evaporation of material from the chromosphere. First, the morphological evidence for the downward-jet interpretation of the strong Hα redshifts is that the downflow region is located directly beneath the X-ray jet and at only a single footpoint. If the downflow were due to chromospheric evaporation, which is dominated by thermal conduction and not energetic electrons (Wülser et al. 1994), redshift

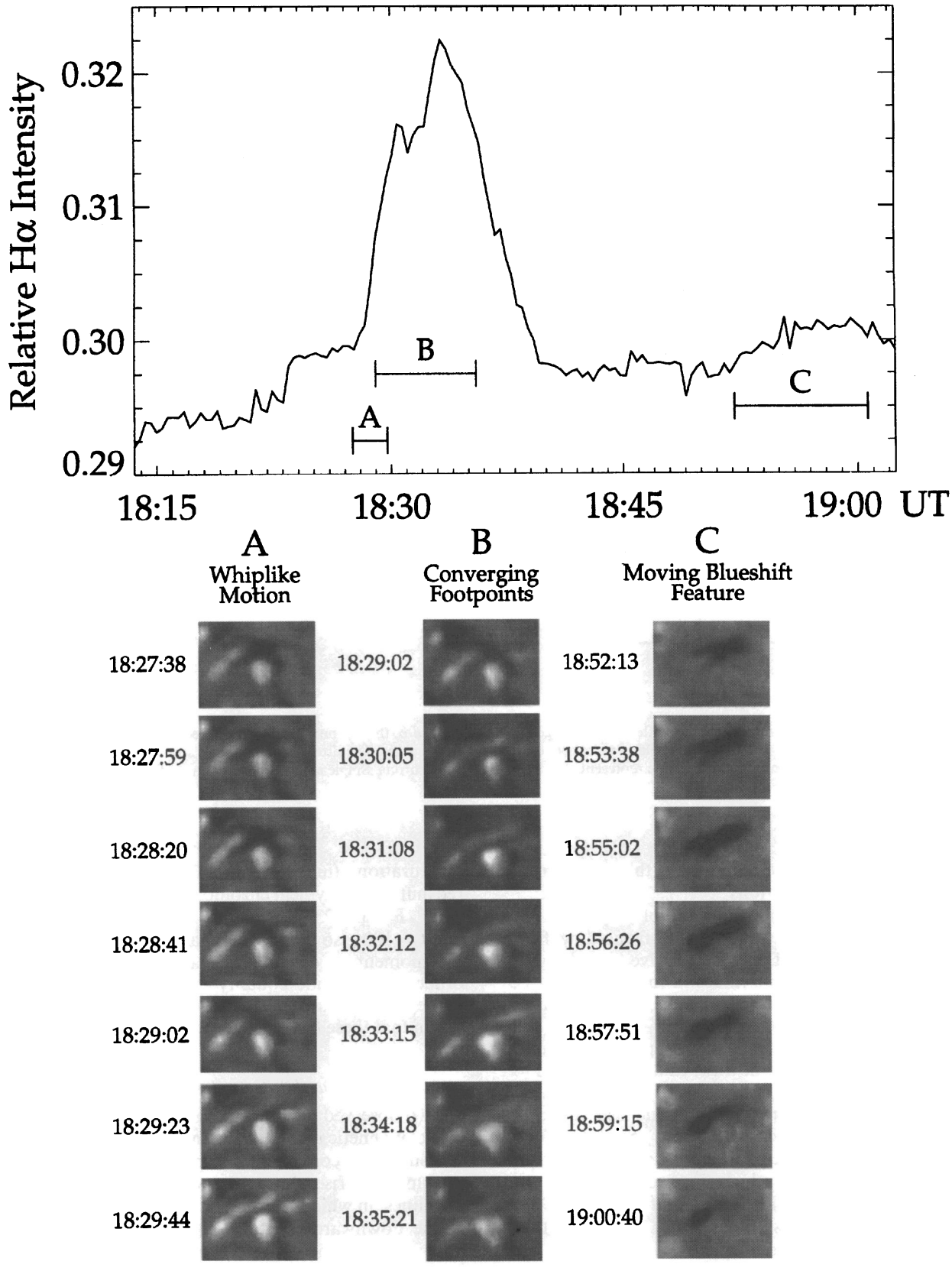

FIG. 9.—Time dependence of phenomena of interest at the base of the jet in the 18:34 event, in the area defined by the black rectangle in Fig. 8. *Top*: Line-center Hα light curve. *Bottom*: Sequences of images. *Sequences A and B*: Hα line–center spectroheliograms. White indicates high intensity, black indicates low. *Sequence C*: Hα Doppler velocity; black indicates blueshift; white, redshift.

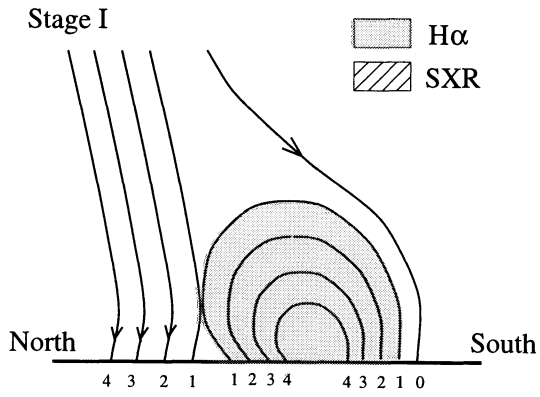

FIG. 10*a*

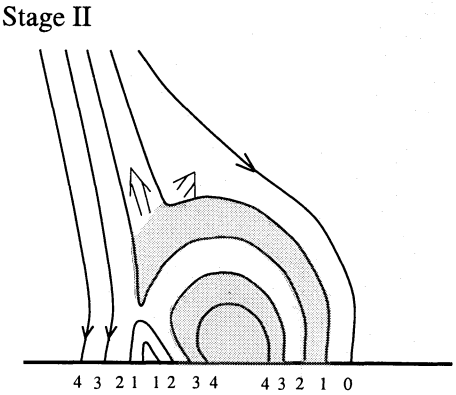

FIG. 10*b*

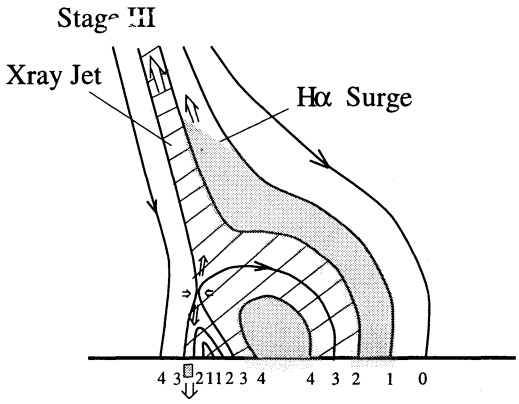

FIG. 10*c*

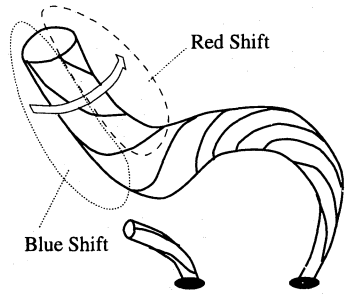

FIG. 10*d*

FIG. 10.—Cartoons of reconnection associated with jets and surges. *Panels a, b, and c*: the temporal evolution of reconnection. Times associated with stages 1, 2, and 3 are shown in Fig. 7. *Panel d*: the role of reconnection in the spin of surges. The directions north and south refer to the 23:11 event; the direction south is toward P0α. The horizontal baseline represents the base of the quiet corona. Single arrows show magnetic field directions; double arrows show mass motions.

regions should appear at *both* footpoints of the north flaring loop, contrary to our observations

Second, the onset times of redshifts and blueshifts are not the same. Large Hα redshift values at the strong-downflow site are delayed by about 1 minute relative to the rapid increase of maximum blueshift values in the surge (Fig. 7). This is suggestive of Forbes' (1986) demonstration (from reconnection models) that the downflow jet out of the reconnection site turns on later than the upflow jet, due to the greater confinement of the downward flow compared to the upward one.

Third, an analysis of momentum content also supports the jet-impact argument. Using the same accretion-shock approach as has been applied to demonstrate momentum balance between upward and downward flows due to chromospheric evaporation in flares (Canfield et al. 1987; Zarro & Canfield 1989), it is straightforward to show that the momentum developed in the Hα downflow is of the same order as that in the X-ray jet that extends above it. Typical values of jet masses are about 10^{13} g, and jet velocities are about 10^{7} cm s^{-1} (Shimojo et al. 1995), implying a typical jet momentum of about 10^{20} g cm s^{-1}. Estimates of the momentum of redshifted Hα material at the base of the surge can be made by deriving its mass from the observed values of the redshifted area A, its maximum velocity v, and the duration t (full width at half-maximum) of the observed redshifts, using typical chromospheric densities $\rho \approx 10^{-11}$ g cm^{-3}. For the 23:11 event, $A = 10^{17}$ cm^2, $v = 10^6$ cm s^{-1}, and $t = 100$ s, so the moving mass $Avt\rho$ is about 10^{14} g, and the momentum developed is about 10^{20} g cm s^{-1}. This order-of-magnitude equality of the momentum developed in the X-ray jet and the Hα downflow supports our interpretation that these flows originate from the same reconnection site.

4.4. *Moving Blueshift Episodes and Converging Footpoints*

Two observed phenomena provide novel evidence for the role of magnetic reconnection in surges and jets: moving Hα blueshifts and converging footpoints. In this interpretation, the blueshift arises during the whiplike transverse motion of field lines on which Hα material is found, starting at the site of the downward-pointing cusp in open field line 1 (just above the reconnection site) and propagating along it to its other end. The converging footpoints arise as reconnection successively proceeds to field lines 1, then 2, then 3 in the bipolar region that is first shown in stage 1.

Are the observed velocities reasonable? As noted above, the measured speed of propagation of the blueshift region (perpendicular to the line of sight) during the period of obvious motion shown in Figure 9 averages 25 km s^{-1} and

peaks at 120 km s^{-1}. Reconnection theory predicts velocities of order 0.1–1.0v_A, where v_A is the Alfvén speed,

$$v_A = B/(4\pi\rho)^{-1/2},$$

or in conventional units,

$$v_A = 300(B/100\ \mathrm{G})/(n_e/10^{12}\ \mathrm{cm}^{-3})^{-1/2}\ \mathrm{km\ s}^{-1},$$

where B is the magnetic field strength, ρ is the mass density, and n_e is the electron number density. For $B = 100$ G and $n_e = 10^{11}$–10^{12} cm^{-3}, v_A ranges from 300 to 1000 km s^{-1}. The gas between field lines 1 and 2 undergoes a whiplike upward motion, as shown by the simulations of Yokoyama & Shibata (1995). Where the opening angle of the reconnected field line at the reconnection point is large, we expect the whiplike motion to proceed at a velocity that is only a fraction of v_A, perhaps 30–100 km s^{-1}. This is of the same order as the moving blueshift observations.

Finally, we note that moving blueshift episodes are often observed well before and well after the times of the X-ray jets, but much less often at the same time. We believe that this simply reflects the temperature sensitivity of our observations. We can detect vertical motions only in Hα (as Doppler shifts). During strong reconnection (stage 3), material on the reconnecting field lines is strongly heated and emits X-rays, not Hα. Hence the moving blueshifts tend not to be observed at the times of the X-ray jets and X-ray loops.

5. CONCLUSIONS

We conclude that the morphology and dynamics of the observed surges and jets require a reconnection model in which magnetic tension and relaxation of twist play an important role. Circumstances favorable to magnetic reconnection are produced by moving satellite sunspots. Strong evidence for reconnection is provided by whiplike motions and the moving blueshift phenomenon, which suggest the slingshot process. Approaching footpoints are a consequence of the reconnection of adjacent loops at successively lower levels in the solar atmosphere. Finally, the spin of the surges is a consequence of the relaxation of stored magnetic twist.

This investigation has been supported by National Science Foundation grants AST 91-15038 and ATM 93-03873, NASA grant NAGW-1542, and NASA contract NAS8-37334. We thank Drs. Terry Forbes, David Rust, and Brigitte Schmieder for interesting discussions, the staff of Mees Solar Observatory for the very useful IVM and MCCD data, and our *Yohkoh* colleagues for their many contributions to building and operating the SXT.

REFERENCES

Blake, M. L., & Sturrock, P. A. 1985, ApJ, 290, 359
Bumba, V. 1960, Publ. Crim. Astrophys. Obs., 23, 212
Canfield, R. C., Metcalf, T. R., Strong, K. T., & Zarro, D. M. 1987, Nature, 326, 165
Forbes, T. G. 1986, ApJ, 305, 553
Foukal, P. 1990, Solar Astrophysics (New York: Wiley), 354
Gaizauskas, V. 1983, in Adv. Space Res., Vol. 2, No. 11, 11
Gu, X. M., Lin, J., Li, K. J., Xuan, J. Y., Luan, T., & Li, Z. K. 1994, A&A, 282, 240
Heinzel, P., & Rompolt, B. 1987, Sol. Phys., 110, 171
Heyvaerts, J., Priest, E. R., & Rust, D. M. 1977, ApJ, 216, 123
Hollweg, J. V., Jackson, S., & Galloway, D. 1982, Sol. Phys., 75, 35
Hyder, C. L., & Lites, B. W. 1970, Sol. Phys., 14, 147
Jefferies, J. T., Lites, B. W., & Skumanich, A. 1989, ApJ, 343, 920
Jefferies, J. T., & Mickey, D. L. 1991, ApJ, 372, 694
Karpen, J. T., Oran, E. S., Mariska, J. T., Boris, J. P., & Brueckner, G. E. 1982, ApJ, 261, 375
Korendyke, C. M., Dere, K. P., Socker, D. G., Brueckner, G. E., & Schmieder, B. 1995, ApJ, 443, 869
Kurowaka, H., & Kawai, G. 1993, in ASP Conf. Ser., 46, The Magnetic and Velocity Fields of Solar Active Regions, ed. H. Zirin, G. Ai, & H. Wang (San Francisco: ASP), 507
Leka, K. D., Canfield, R., McClymont, A. N., & van Driel–Gesztelyi, L. 1996, ApJ, in press (Paper II)
Leka, K. D., van Driel–Gesztelyi, L., Nitta, N., Canfield, R. C., Mickey, D. L., Sakurai, T., & Ichimoto, K. 1994, Sol. Phys., 155, 301 (Paper I)
Livshits, M. A., & Pikel'ner, S. B. 1964, Soviet Astron.–AJ, 8, 368
Mickey, D. L., Canfield, R. C., LaBonte, B. J., Leka, K. D., & Metcalf, T. R. 1996, Sol. Phys., submitted
Ogawara, Y., et al. 1991, Sol. Phys., 136, 1
Öhman, Y., Hosinsky, G., & Kusoffsky, U. 1968, in Proc. Nobel Symp. 9, Mass Motion in Solar Flares and Related Phenomena, ed. Y. Öhman (New York: Wiley; Stockholm: Alqvist & Wiksell), 95
Penn, M. J., Mickey, D. L., Canfield, R. C., & LaBonte, B. J. 1991, Sol. Phys., 135, 163
Pikel'ner, S. B. 1969, Soviet Astron.–AJ, 13, 259
Roy, J.-R. 1973a, Sol. Phys., 28, 95
———. 1973b, Sol. Phys., 32, 139
Rust, D. M. 1968, in IAU Symp., 35, Structure and Development of Solar Active Regions, ed. K. O. Kiepenheuer (Dordrecht: Reidel), 77
Rust, D. M., Webb, D. F., & MacCombie, W. 1977, Sol. Phys., 54, 53
Sakao, T., et al. 1992, PASJ, 44, L111
Schmahl, E. J. 1981, Sol. Phys., 69, 135
Schmieder, B., Golub, L., & Antiochos, S. K. 1994, ApJ, 425, 326
Schmieder, B., Shibata, K., van Driel–Gesztelyi, L., & Freeland, S. 1995, Sol. Phys., 156, 245
Schmieder, B., van Driel–Gesztelyi, L., Gerlei, O., & Simnett, G. 1993, Sol. Phys., 146, 163
Shibata, K., Nishikawa, T., Kitai, R., & Suematsu, Y. 1982, Sol. Phys., 77, 121
Shibata, K., et al. 1992a, PASJ 44, L173
Shibata, K., Nozawa, S., & Matsumoto, R. 1992b, PASJ, 44, 265
Shibata, K., & Uchida, Y. 1986, Sol. Phys., 103, 299
Shibata, K., Yokoyama, T., & Shimojo, M. 1994, in New Look at the Sun with Emphasis on Advanced Observations of Coronal Dynamics and Flares, ed. S. Enome & T. Hirayama, NRO Rep., 360, 75
Shimojo, M. 1994, B.S. thesis, Dept. of Phys., Tokai Univ. (in Japanese)
Shimojo, M. Shibata, K., Hashimoto, T., & Hirayama, T. 1995, in IAU Colloq. 153, Magnetodynamic Phenomena in the Solar Atmosphere, ed. Y. Uchida, T. Kosugi, & H. S. Hudson, in press
Steinolfson, R. S., Wu, S. T., & Schmahl, E. J. 1979, Sol. Phys., 63, 187
Sterling, A. C., Shibata, K., & Mariska, J. T. 1993, ApJ, 407, 778
Svestka, Z. 1976, Solar Flares (Dordrecht: Reidel)
Svestka, Z., Farnik, F., & Tang, F. 1990, Sol. Phys., 127, 149
Tandberg-Hanssen, E. 1977, in Illustrated Glossary for Solar and Solar-Terrestrial Physics, ed. A. Bruzek & C. J. Durrant (Dordrecht: Reidel), 106
Tsuneta, S., et al. 1991, Sol. Phys., 136, 37
Uchida, Y. 1969, PASJ, 21, 128
Wülser, J.-P., et al. 1994, ApJ, 424, 459
Yokoyama, T., & Shibata, K. 1994, in New Look at the Sun with Emphasis on Advanced Observations of Coronal Dynamics and Flares, ed. S. Enome & T. Hirayama, NRO Rep., 360, 367
———. 1995, Nature, 375, 42
Xu, A., Ding, J., & Yin, S. 1984, Chinese Astron. Astrophys., 8, 294
Zarro, D. M., & Canfield, R. C. 1989, ApJ, 338, L33
Zirin, H. 1988, Astrophysics of the Sun (Cambridge: Cambridge Univ. Press)